Published in final edited form as:
NMR Biomed. 2012 February ; 25(2): 236–246. doi:10.1002/nbm.1737.

Accurate noninvasive measurement of cell size and compartment shape anisotropy in yeast cells using double-PFG MR

Noam Shemesh[1], **Evren Özarslan**[2,3], **Peter J Basser**[2], and **Yoram Cohen**[1,*]

[1] School of Chemistry, The Raymond and Beverly Sackler Faculty of Exact Sciences, Tel Aviv University, Tel Aviv 69978 Israel

[2] Section on Tissue Biophysics and Biomimetics, PPITS, NICHD, National Institutes of Health, Bethesda, Maryland 20892, USA

[3] Center for Neuroscience and Regenerative Medicine, USUHS, Bethesda, Maryland 20892, USA

Abstract

Accurately characterizing pore morphology is of great interest in a wide range of scientific disciplines. Conventional single-Pulsed-Field-Gradient (s-PFG) diffusion MR can yield compartmental size and shape only when compartments are coherently ordered using the *q*-space approaches that necessitate strong gradients. However, the double-PFG (d-PFG) methodology can provide novel microstructural information even when specimens are characterized by polydispersity in size and in shape, and even when anisotropic compartments are randomly oriented. In this study, for the first time, we show that angular d-PFG experiments can be used to accurately measure cellular size and shape anisotropy of fixed yeast cells using relatively weak gradients. The cell size, as measured by light microscopy was found to be 5.32±0.83 μm, while the results from the non-invasive angular d-PFG experiments yielded a cell size of 5.46±0.45 μm. Moreover, the low shape anisotropy of the cells could be inferred from experiments conducted at long mixing times. Finally, similar experiments were conducted in a phantom comprised of anisotropic compartments that were randomly oriented, showing that angular d-PFG MR provides novel information on compartment eccentricity that could not be accessed using conventional methods. The angular d-PFG methodology seems promising for accurate estimation of compartment size and compartment shape anisotropy in heterogeneous systems in general and biological cells and tissues in particular.

Keywords

Cell size; cell shape; diffusion; NMR; double-PFG; yeast cells; compartment shape anisotropy; microscopic anisotropy

Introduction

Application of pulsed-field-gradients (PFGs) can directly sensitize the magnetization arising from NMR-observable nuclei to molecular displacement, thereby enabling manifestation of diffusion processes in the NMR signal decay (1). Endogenous fluids undergoing restricted diffusion within pores and interstices of porous media can be used as excellent reporters on

*Corresponding author: Prof. Yoram Cohen, School of Chemistry, The Raymond and Beverly Sackler Faculty of Exact Sciences, Tel Aviv University, Ramat Aviv, Tel Aviv 69978, Israel, ycohen@post.tau.ac.il, Tel/fax- 972 3 6407232/972 3 6407469.

geometrical features of the restricting milieu, enabling non-invasive characterization of important microstructural information in many opaque systems such as neuronal tissues (2), isolated cells (3), porous materials (4) and even rocks (5).

Conventional single-PFG (s-PFG) diffusion MR methods employ a single pair of diffusion gradient vectors **G** with duration δ, which are separated by a diffusion period Δ. The important quantity characterizing the diffusion weighting is the wavevector **q**, where $\mathbf{q}=(2\pi)^{-1}\gamma\delta\mathbf{G}$. Conventional s-PFG approaches are useful for obtaining compartment size especially when monodisperse pores are coherently organized using the diffusion-diffraction phenomenon (6). When monodisperse pores are anisotropic and coherently placed, the diffusion-diffraction patterns are also extremely sensitive to compartment orientation, thus offering information on anisotropy of the coherently organized compartments (7). Indeed, diffusion-diffraction experiments were conducted on various systems including RBCs (8,9), narrowly distributed emulsions (10), and even on single crystals using electron spin resonance (ESR) (11). However, these diffusion-diffraction patterns vanish in more heterogeneous specimens characterized by size polydispersity and/or orientation distributions. In such cases the *q*-space approach (12,13) can then be used to estimate compartment sizes. The *q*-space approach entails sampling the normalized signal decay, E(*q*) up to high *q*-values and then Fourier transforming the data. The resulting displacement probability distribution functions (PDFs) can be used to estimate the displacement profile in a given component (14). While the utility of size contrast has been shown in the past in many applications (15–18), recent ex-vivo q-space imaging (QSI) studies of the spinal cord employing very high *q*-values using extremely strong gradients provided striking evidence suggesting that size contrast can provide “virtual histology” (19,20). However, these striking results were obtained using extremely strong gradient pulses. In addition, relatively many *q*-values need to be collected thus rendering the methodology rather demanding.

Diffusion Tensor Imaging (DTI) (2), which is conducted at lower *q*-values, can be used to infer on ensemble anisotropy (EA) when anisotropic compartments are coherently organized; indeed, DTI is used with great success to depict white matter microstructure and to perform fiber tracking in the CNS (21). However, another significant drawback of s-PFG methodologies is that they fail to accurately depict compartment anisotropy when eccentric compartments are randomly oriented since the local diffusion directors are completely averaged within the excited volume, creating macroscopic isotropy.

The double-PFG (d-PFG) methodology is emerging as a novel means to overcome these inherent limitations of s-PFG NMR. The d-PFG sequence (22) is an extension of s-PFG, employing an additional pair of diffusion sensitizing gradients. The d-PFG sequence therefore, spans a large parameter space, including the gradient vectors $\mathbf{G_1}$ and $\mathbf{G_2}$, their respective durations δ_1 and δ_2, and the diffusion periods each gradient pair spans, namely Δ_1 and Δ_2 (Figure 1A). Another important parameter unique to d-PFG MR is the duration between the two diffusion periods, namely the mixing time (t_m), which can either have a finite value (Figure 1A) or can be set to zero (Figure 1B). Early d-PFG work focused on comparing the signal decay up to high *q*-values when $\mathbf{G_1}$ and $\mathbf{G_2}$ were either parallel or perpendicular, thus offering a glance towards the eccentricity of compartments such as yeast cells (22,23), liquid crystals (24) and even in grey matter and spinal cord in MR imaging (25,26); other early d-PFG experiments focused on different acquisition schemes such as two dimensional diffusion-diffusion correlation approaches (27,28).

Two unique features of d-PFG, which have no parallel or analogue in s-PFG MR, are the angle Ψ between the two gradient pairs $\mathbf{G_1}$ and $\mathbf{G_2}$, and the mixing time between diffusion periods which can be combined to devise the angular d-PFG methodology, first suggested theoretically by Mitra (29). In this methodology, the orientation of $\mathbf{G_1}$ is set in a certain

direction, and the orientation of $\mathbf{G_2}$ is varied along the angle Ψ (Figure 2A) while keeping the diffusion periods, mixing time and the q-value for this angular d-PFG experiment constant (in the angular d-PFG experiment $|\mathbf{q}|=|\mathbf{q}_1|=|\mathbf{q}_2|$, where $\mathbf{q}_i=((2\pi)^{-1}\gamma\delta\mathbf{G}_i)$, i.e. the magnitude of the gradients is kept constant and equal). The d-PFG NMR diffusion signal as a function of Ψ (hereafter referred to as E(Ψ)) at a given *q*-value and mixing time was predicted to give rise to angular dependencies that offer novel and unique microstructural information. When diffusion is restricted, the angular dependence at t_m=0 ms was theoretically predicted to yield a bell-shaped function, from which the pore size could be measured; importantly, these bell shaped functions were predicted even at *low q-values* (where $2\pi q$*a<1, where 'a' is the pore dimension) thus offering a novel means for size measurements using mild gradient conditions (29). Considering the potential of compartment size as a useful source of contrast in CNS tissues, this could be important since *q*-space approaches necessitate very high q-values to be reached, i.e. strong gradients need to be implemented (especially in light of the need to fulfill the short gradient pulse (SGP) approximation in these approaches).

Recent theoretical advances provided exact solutions to the diffusion attenuated MR signal decay for arbitrary timing parameters (30,31), and subsequently the theory was extended beyond the $2\pi q$a<1 regime to a general framework for diffusion in NMR (32). Further theoretical progress (33) suggested that besides compartment size, compartment shape anisotropy can also be obtained from d-PFG MR conducted at different mixing times since different anisotropy mechanisms contribute to the NMR signal at different mixing times (t_m): at *short* t_m, the d-PFG NMR signal comprises contributions from (1) microscopic anisotropy (μA), (2) compartment shape anisotropy (e.g. the deviation of pores from perfect spheres), and (3) ensemble anisotropy (EA, the coherence of packing of anisotropic pores) (for a general treatment of these scenarios see (33)). Therefore, the angular d-PFG MR experiment can depict microscopic anisotropy at short t_m as long as restricted diffusion occurs, regardless of the compartment anisotropy and organization. By contrast, at *long* mixing times, the effects of μA are decoupled from the signal, and therefore only compartment shape anisotropy dominates the angular dependence even when anisotropic compartments are randomly oriented (Figure 2B) or spherical (Figure 2C). The result is that for spherical compartments (Figure 2C), which are isotropic, no Ψ-dependence is predicted resulting in a flat E(Ψ) profile, while for locally anisotropic pores that are randomly oriented (Figure 2B), modulated curves that depend solely on compartment eccentricity were predicted (33). Although the modulation in E(Ψ) was not predicted to afford refined information on the actual pore shape (for example cylinders and ellipsoids of the same length and radius would yield similar E(Ψ) modulations (33)), the ability to infer on the presence on the anisotropy on the microscopic scale in the absence of EA implied that angular d-PFG MR can be of importance in characterizing randomly oriented porous media and biological tissue. It should be noted that in case EA exists, it can also be detected in the long t_m regime.

While E(*q*) d-PFG MR measurements using collinear and orthogonal gradient vectors were performed previously up to high *q*-values, showing that compartment shape could be inferred in yeast cells (23) and in liquid crystals (24), the bell shaped E(Ψ) dependencies were only recently observed experimentally at low q-values in both MR spectroscopy (34) and in MR imaging experiments (35,36), and the effect of experimental parameters on the bell shaped functions was studied and accounted for (34), even when a freely diffusing component was included (37). Very recently, the modulated E(Ψ) curves at long t_m were experimentally observed for the first time in a controlled system containing a porous medium comprised of randomly oriented cylindrical pores (37) using bipolar-d-PFG MR sequences (Figure 1C–D) that are preferable when severe susceptibility effects are present. Other simulations support the idea that angular d-PFG MR can yield novel microstructural

information: notably, a tensor approach to angular d-PFG NMR was introduced, where rotationally invariant measures of anisotropy could be extracted (38–41). In previous studies, controlled specimens in which the ground-truth was known *a-priori* were used to challenge the theoretical framework in terms of accuracy and robustness of the extracted microstructural information, yielding excellent agreement between experiments and theory at both low (34,37,42) and high *q*-values (42–44). In light of the previous findings, we sought to challenge the ability of angular d-PFG to extract microstructural information in a real biological specimen. We therefore performed the angular d-PFG experiments in fixed yeast cells, previously used to study intracellular diffusion coefficients (45), exchange (46) and restricted diffusion (47). The objectives of the present study were to test the viability of angular d-PFG MR as a new means to report on cellular morphology (size and shape) in such a realistic specimen non-invasively, and furthermore, to challenge the accuracy of the results; to challenge the possibility of doing so using relatively weak gradients; and to explore the possibility of contrast between spherical and non-spherical compartments that are randomly oriented, i.e. scenarios where there is no EA.

Materials and Methods

Theory and data analysis

The compartment size measurements were based on the general theoretical framework for diffusion in MR presented in (32) and in (33). In this method, a general MR gradient waveform is expressed as a piecewise constant function. Each pulse in the acquisition is represented by a vector whose components are infinite-dimensional matrices. The effect of each pulse is then expressed as the exponential of one such matrix. The technique makes it possible to obtain an analytical expression for the diffusion-related MR signal attenuation with relative ease. The analytical expression is exact for piecewise constant gradient waveforms, whereas accurate approximations can be obtained when slowly varying gradients are employed. The reader is referred to (32) for a detailed description of the method, which makes it possible to compute the effect of restricted diffusion efficiently and accurately. The E(Ψ) are fitted to curves predicted by the theory assuming a specific compartment shape anisotropy to extract compartment size. Note that the assumption on compartment shape anisotropy is based on the observations at long t_m measurements. In analyzing the data obtained from the yeast cells, a spherical geometry was assumed based on the observations of double-PFG measurements with long mixing times (*vide infra*). In the phantom, such measurements indicated the presence of compartment shape anisotropy, and therefore an infinite cylinder model was employed. Based on the single-PFG measurements that yielded no ensemble anisotropy, the cylinders were assumed to be randomly distributed. When there is a continuous distribution of cylinders, one needs to evaluate an integral over a sphere spanned by all orientations of the (infinitely long or capped) cylinders. This integral, which takes into account the orientational averaging of the cylinders, can be evaluated by employing an iterated Gaussian quadrature technique. In our implementation, we used such a scheme with 48 transformation points. A Levenberg-Marquardt algorithm was employed using the MPFIT package in IDL (provided at http://www.physics.wisc.edu/~craigm/idl/fitting.html). The uncertainty of each data point was assumed to be 1%, and the extracted values are reported as mean±SD. A bicompartmental model (37) was fitted to the data sets from both specimens to account for the effects of a freely diffusing component, as the presence of Gaussian diffusion affects the signal decay both along the *q*-axis as well as along the Ψ-axis (37). However, for the yeast cell data set, different values for bulk diffusivity were allowed for the extracellular and intracellular spaces.

The E(Ψ) datasets from the yeast cells (but not the phantom, *vide infra*) were additionally fitted to Mitra's theory (29) so that the microstructural information obtained could be

compared between a method that assumes the SGP approximation (29) and the new theory that takes the finite gradient lengths into account in the angular d-PFG experiments (32, 33).

Experimental

Specimen preparation

Yeast cells—~1.5 gr of commercially available dry *S. Cerevisiae* were hydrated with ~40 ml of PBS. The mixture was vortexed for several minutes and subsequently centrifuged at 1000 rpm for 10 minutes. The supernatant fluid was decanted, and ~40 ml of 4% paraformaldehyde (Sigma Aldrich) were added to the pellet. The yeast cells were vortexed and then immersed in the paraformaldehyde for 90 minutes and then centrifuged at 1200 rpm for 10 minutes. The supernatant was again removed, and the fixed cells were washed twice with PBS and centrifuged at 1200 rpm. No bubbling or activity could be visually detected after fixation. Finally, the 0.6 gr of fixed yeast pellet was hydrated with 800 μl of PBS, vortexed and transferred to the NMR tube.

The fixed yeast cells were allowed to settle in the NMR tube overnight at 4oC, and a small portion of water that collected on top of the yeast was aspirated prior to the NMR experiments.

Randomly oriented cylinders—The preparation of such controlled porous media was described previously (42). Briefly, water-filled microcapillaries with well known inner diameter of 29±1 μm were first cut to macroscopic ~5–10 mm long pieces which were briefly dried externally. Subsequently, these microtubes were crushed by mechanical force to very small dust-like particles which were re-immersed in water for several days for filling. The resulting porous medium was carefully dried externally and placed in an 8 mm NMR tube filled with Fluorienert. Owing to density and polarity differences between water and Fluorinert, any water residue on the outer portion of the crushed microcapillaries floated to the top of the NMR tube, outside the receiver coils, while the water within the inner diameter of the crushed microcapillaries were trapped in the intratubular space. Owing to their macroscopic small size, the pores assumed a completely random orientation while retaining their cylindrical geometry with ID=~29±1 μm and axial dimension on the order of ~100–800 μm (42).

NMR experiments

The NMR experiments were conducted in an 8.4 T Bruker NMR spectrometer, equipped with a Micro5 probe capable of producing nominal pulsed gradients up to 1900 mT/m in the x-, y- and z-directions. Constant temperature was kept throughout the experiments at T=303K. All specimens were allowed to equilibrate with the magnet temperature for at least an hour prior to the NMR experiments.

For both fixed yeast cells and phantom, the methodology of angular d-PFG MR experiments was performed as previously published (34,37,42). Briefly, $\mathbf{G_1}$ was set in the x-direction, and the orientation of $\mathbf{G_2}$ was varied in the X-Y plane along 25 different values of Ψ (Figure 2A) Note that in these angular d-PFG experiments the mixing time, diffusion and gradient magnitude are kept constant for each E(Ψ) profile. The only variant is the relative angle between the gradient vectors Ψ. The magnitude of the gradients are kept constant, e.g. $|\mathbf{G_1}|=|\mathbf{G_2}|$, resulting in $|\mathbf{q_1}|=|\mathbf{q_2}|=|\mathbf{q}|$ for each E(Ψ) profile.

Yeast cells—Single-PFG experiments were performed using a stimulated echo sequence employing bipolar gradients (bp-s-PFG). Experiments were performed in the x-, y- and z-

directions with the following parameters: 48 *q*-values were collected with G_{max}=1600 mT/m and Δ/δ=200/3 ms, resulting in a q_{max} of 2043 cm^{-1}.

Another s-PFG experiment (with conventional monopolar gradients) was performed for the *q*-space analysis with the following parameters: 96 *q*-values were collected with G_{max}=1600 mT/m and Δ/δ=50/2 ms, resulting a q_{max} of 1362 cm^{-1}.

The conventional angular double-PFG experiments were performed with the sequence shown in Figure 1B, with the following parameters: eight *q*-values were collected with G=25, 136, 246, 357, 468, 579, 689 and 800 mT/m with $\delta_1=\delta_2=\delta_3$=2 ms, resulting in *q* values of 21.3, 115.8, 209.4, 304, 398.5, 493, 586.5 and 681.3 cm^{-1}, respectively, and with $\Delta_1=\Delta_2$=250 ms and t_m=0 ms. The bipolar d-PFG (bp-d-PFG) experiments were performed with sequences shown in Figure 1C–D. For the t_m=0 ms, the sequence shown in Figure 1D was used. Ten *q*-values were collected with values of 25, 111, 197, 283, 369, 456, 542, 628, 714 and 800 mT/m and $\delta_1=\delta_2=\delta_3$=3 ms, resulting in *q* values of 32, 141.8, 251.6, 361.5, 471.4, 582.5, 692.3, 802.2, 912, and 1021.9 cm^{-1}, respectively, and with $\Delta_1=\Delta_2$=200 ms. For the finite mixing time experiments, the sequence shown in Figure 1C was used with exactly the same parameters except $\delta_1=\delta_2$=3 ms, and t_m was set to 8.4, 11.4 and 19.4 ms.

Randomly oriented cylinders—The bipolar s-PFG sequence was performed in the x-, y- and z-directions using the following parameters: 32 *q*-values were collected with G_{max}=800 mT/m and Δ/δ=250/3 ms, resulting in a q_{max} of 1021.5 cm^{-1}.

The bipolar d-PFG (bp-d-PFG) experiments were performed with sequences shown in Figure 1C–D. For the t_m=0 ms, the sequence shown in Figure 1D was used. Seven *q*-values were acquired with gradients of 25, 54, 83, 112, 142, 171 and 200 mT/m and with $\delta_1=\delta_2=\delta_3$=2.6 ms, resulting in *q* values of 27.6, 59.8, 91.9, 124, 157.2, 189.3 and 221.4 cm^{-1}, respectively, and with $\Delta_1=\Delta_2$=250 ms. For the finite mixing time experiments, the sequence shown in Figure 1C was used with exactly the same parameters except $\delta_1=\delta_2$=2.6 ms, and experiments with t_m of 7.6, 10.6, 18.6, 53.6 and 103.6 ms were acquired.

Light microscopy

The fixed yeast cells were taken from the NMR tube after the NMR experiments, diluted 1:50 in PBS, and placed on a coverslip. To capture images of the fixed yeast cells, an Olympus IX71 microscope was used with x60 amplification.

Quantification of cellular size from microscopy images

Fifteen separate microscope images were imported to ImageJ software (NIH, Bethesda, Maryland, USA, http://rsb.info.nih.gov/ij/), and a threshold was set such that cells were demarcated from their neighbors optimally. The Feret radius (longest distance within a domain) was automatically measured for ~900 cells. After inspection of the yeast cell size visually, Feret radii smaller than 3 μm or larger than 7 μm were excluded from the analysis since the ImageJ analysis takes parts of cells or tends to clamp cells together as one object, respectively. The histograms of the cells were then plotted, from which the mean cell size ±SD was extracted. The analysis of the NMR results was completely blinded from the size extracted by microscopy.

Size extraction from single-PFG *q*-space experiment

The *q*-space analysis was performed only for the yeast cells specimen since in the randomly oriented cylinders phantom the analysis would be much less accurate owing to the lack of EA. The E(*q*) data were Fourier transformed, affording the displacement probability distribution function (PDF). The PDF was then fitted to a bi-Gaussian function, assuming

one fast diffusing component and one slow diffusing component. The full width at half maximum (FWHM) of each Gaussian was used to obtain the rmsd of each component (15,16).

Results

To determine if diffusion in the yeast cells specimen is anisotropic (i.e. whether EA exists), we conducted bipolar s-PFG (bp-s-PFG) NMR experiments in the x-, y- and z-directions. The bipolar gradients were used to ensure that susceptibility effects do not cause any directional preference. Figure 3A shows the data from these experiments. An isotropic signal decay was observed, suggesting that there is no EA present within the yeast cells specimen. However, this information is not sufficient to infer whether the cells are spherical or anisotropic but randomly oriented since in both cases, similar isotropic profiles will be obtained. Indeed, Figure 3B shows a similar isotropic decay in the control phantom comprised of randomly oriented water-filled cylindrical compartments having nominal inner diameter of 29±1 μm, demonstrating the limitation of s-PFG MR to distinguish between the two scenarios depicted in Figure 2B and 2C.

To obtain further microstructural information on the local cellular shape we performed angular bp-d-PFG experiments with increasing t_m for both yeast cells and the control phantom (Figure 4). The E(Ψ) profile from the yeast cells at t_m=0 ms and at $2q$=531 cm^{-1} can be seen in Figure 4A. An angular dependence in the form of a bell shaped function can be readily observed, and the signal rises between Ψ=0o and Ψ=180o by about 10%, subsequently declining back to its original value at Ψ=360o. It should be noted that the SNR of the NMR signal in the yeast cells was more than 1000 even at the highest q-values employed in this study. Importantly, this E(Ψ) angular dependence already bears important microstructural information: it unequivocally demonstrates the presence of μA, arising solely from restricted diffusion. However, to allow effects of compartment shape anisotropy to become accentuated, long mixing times are needed (33). In the fixed yeast cells, already at a relatively short value of t_m=8.4 ms, the angular profile becomes flat and remains flat for increasing values of t_m (Figure 4A). Such a flat profile at long t_m is expected for spherical compartments and was observed for all *q*-values (data not shown).

In the control phantom however, where anisotropic compartments were randomly oriented, several interesting phenomena were observed. Figure 4B shows E(Ψ) plots for various mixing times at $2q$=181 cm^{-1} using the bp-d-PFG sequences shown in Figures 1C–D. At t_m=0 ms, the E(Ψ) profile was somewhat different compared to the E(Ψ) profile at t_m=0 ms in the yeast cells, with the bell-shaped curve exhibiting slight modulations (at higher *q*-values these modulations were much more pronounced, data not shown). Moreover, a very pronounced modulation in the E(Ψ) signal was observed for all non-zero values of t_m, showing a decrease between E(Ψ=0°) and E(Ψ=90°) of ~20% before subsequently rising back towards E(Ψ=180°). This behavior was then mirrored up to Ψ=360°.

These results unambiguously demonstrated that although there was no EA in both yeast cells and phantom, the local anisotropy, or eccentricity, of the yeast cells is very low while the pores in the synthetic porous phantom are in fact anisotropic, randomly oriented compartments. Thus, these long t_m measurements offered insight into what geometrical model could be used in the compartment size analysis: the flat E(Ψ) dependence implied that a spherical model could be used for extracting cellular size in the yeast cells, while the modulated E(Ψ) in the control phantom implied that an infinite cylindrical model could be used for the synthetic phantom.

Figure 5 shows a representative light microscopy image, showing the morphology of the yeast cells. The microscopy images clearly revealed that the yeast cells were indeed mostly spherical, with negligible eccentricity, validating the non-invasive long t_m angular d-PFG MR results. Figure 5B shows the quantification of the yeast cell size. The average±SD cellular size that was measured was 5.32±0.83 μm.

Figure 6A shows the E(Ψ) data from an angular d-PFG experiment at t_m=0 ms (symbols) for fixed yeast at 3 different *q*-values, along with the fitting to the theory (solid lines). Clearly, the theoretical fit to the experimental data shows remarkable correspondence. It should be noted that the plateau-like feature that can be seen in the experimental data at higher *q*-values is a slight susceptibility artifact that was corrected when bipolar gradients were used (data not shown). The size that was extracted from the fitting of the theory to the experimental angular d-PFG data was 5.46±0.45 μm (R^2=0.979). Moreover, when angular bp-d-PFG measurements in which the violation of the short gradient pulse approximation is more pronounced were performed on the yeast cells with t_m=0 ms, the size that was extracted using the general framework in (33,32) didn't vary significantly, and was found to be 5.37±0.22 μm (R^2=0.999). Note that the datasets were analyzed completely blindly, with no a-priori knowledge of compartment size or even on the expected length scales within the specimen.

We also applied Mitra's theory (29) to extract the compartment size. The cellular size that was extracted using this approach in the angular d-PFG experiments was 4.31±0.06 μm, or about 20% lower compared to the size measured microscopy. When Mitra's theory was employed to extract compartment size from the bp-d-PFG dataset, a much smaller size of 3.23±0.04 μm was obtained, more than 40% smaller than the size measured from microscopy.

Figures 6B shows the E(Ψ) plots obtained from angular bp-d-PFG at t_m=0 ms for three *q*-values in the randomly oriented cylinders. Here, bipolar gradients are imperative for compensating for severe susceptibility effects in the specimen (37). The symbols represent the experimental data while the solid curves represent the fits to the theory. Based on the pronounced E(Ψ) modulation in Figure 4B at long t_m, we used the infinite cylinder model for this specimen. The size that was extracted for the phantom was 27.06±0.22 μm (R^2=0.926), in good agreement with the nominal inner diameter.

To compare the d-PFG size measurements with the microstructural information that can be obtained using the conventional s-PFG methods, a *q*-space experiment (12,13) was performed on the yeast cells specimen. The displacement PDF obtained from the Fourier transform of the E(*q*) was fitted to a bi-Gaussian function, and two components were extracted (15,16). The rmsd of the slow component was 3.85±0.15 μm. Again, the size extracted is smaller than the nominal cell size measured from the invasive microscopy images.

Discussion

Accurate measurements of morphological features such as compartment size and shape are desirable in many areas of research that require a "fingerprint" of the optically turbid specimen. In biological applications, cell size and shape are of great significance from characterization of cellular processes (9,48) to delineation of different healthy (19,20) and diseased regions (49,50) owing to size contrast.

To determine the compartment dimension, most applications use the conventional s-PFG approaches ranging from diffusion-diffraction (6) or *q*-space MR (12,13) to more sophisticated methods for determining length scales (5,51–53). However, among the

inherent limitations of the diffusion-diffraction approaches is that a-priori knowledge of the pore shape is needed to obtain accurate sizes (54); furthermore, when *q*-space approaches are used to obtain the rmsd the information on pore shape will not be available unless EA exists. Additionally, the demand for very strong gradient amplitudes poses both a technological constraint (as it is currently relatively difficult to manufacture three dimensional strong gradient systems) as well as a methodological limitation (since SNR at very high *q*-values tends to be low). Finally, in many instances in biophysical applications, the diffusion modes within the specimen are hard to infer, for example assignment of water to intra/extra spaces is controversial in many tissues in the CNS (55,56).

Previous studies on angular d-PFG MR, which is emerging as a valuable means for obtaining novel microstructural information in settings where conventional s-PFG methods are limited (i.e. when there is no coherent organization of compartments), were mainly focused on validating the methodology and challenging the microstructural information that could be obtained from well-controlled phantoms, where a-priori knowledge of the ground truth was a major advantage (34,37,42–44). Based on the foundations laid by the former studies in controlled specimens, we applied the angular d-PFG methodology in yeast cells, and also in another phantom where no EA exists. It should be noted that yeast cells were also the substrate of the first published d-PFG study, which employed high *q*-values d-PFG measurements to infer on the eccentricity of irradiated yeast cells (22). Further studies in yeast cells (23) and liquid crystals (24), demonstrated that that indeed some information on locally anisotropic motions within randomly oriented specimens could be inferred from comparing E(q) signal decays (up to high q-values) in collinear and orthogonal (non-angular) d-PFG MR.

The main goals of this study were to measure accurate compartment size in the yeast cells and to infer on the additional morphological information that can be obtained on compartment eccentricity. Before one can attempt to extract accurate cellular size, some knowledge on the underlying anisotropy of the cells and their organization needs to be determined so that a suitable model can be selected for the size analysis. Since macroscopically, both yeast cells and randomly oriented cylinders specimens exhibit isotropic diffusion, the bp-s-PFG experiments yielded isotropic signal decay, demonstrating that bp-s-PFG experiments cannot distinguish between these diffusion scenarios, for which EA is not present. The angular d-PFG MR, on the other hand, can manifest the effects of anisotropy on a microscopic scale owing to restriction (μA), which could be used to infer on the compartment size, as well as effects of compartment shape anisotropy that arise from compartment eccentricity, even at low q-values. Therefore, angular d-PFG MR has the potential to report on the compartment size and compartment shape anisotropy. While the bp-s-PFG MR experiments did not report on underlying microstructure, we demonstrated here for the first time that the E(Ψ) plots at long t_m in angular bp-d-PFG experiments in fact provide shape contrast between spherical yeast cells and the randomly oriented cylindrical compartments based on their respective compartment eccentricity: the spherical cells exhibited a Ψ-independent angular dependence at long t_m, while the randomly oriented cylinders exhibited a marked modulation of the E(Ψ) plots, both phenomena predicted by the theory (33). It should be noted that although one can infer on compartment shape anisotropy when E(Ψ) curves appear modulated and estimates for compartment eccentricity can be obtained (33), it is practically not possible to distinguish between compartments having similar eccentricities but different shapes, such as ellipsoids and capped cylinders. This means that the fine details of the geometry would be difficult to resolve in angular d-PFG NMR at long t_m. However, although the exact *shape* of the pore cannot be measured, the shape *anisotropy* is available from the long t_m angular d-PFG NMR. Such estimates on the eccentricity of the compartments are important novel microstructural information that is unavailable from s-PFG MR. It seems therefore that the angular d-PFG MR methodology

offers indeed novel microstructural information on the underlying compartment morphology.

While the modulation in the E(Ψ) curve owing to compartment shape anisotropy at long t_m has been shown recently for the first time (42), here we also studied the t_m dependence in a sequence that employed z-storage of magnetization during most of the mixing time. Such t_m dependent measurements could be important especially when there is a distribution of length scales, to ensure that μA has been completely decoupled albeit not introducing further T_2 weighting with increasing t_m. Interestingly, we find that even relatively short t_m is sufficient to decouple μA from compartment shape anisotropy even in relatively large compartments when bp-d-PFG is used, probably owing to an effective mixing time that is induced in the bp-d-PFG sequence during the time between the split gradients. It should be noted that it is possible to attempt to extract compartment size even at the long t_m regime; however, since the information on μA is lost at long t_m and a Ψ-independent curve was obtained for the yeast cells, the fitting would amount to no more than fitting multiple, but identical E(q) profiles, thereby the useful additional dimension that is provided by the angle Ψ to infer on μA is not fully exploited.

Once the compartment shape anisotropy is non-invasively determined, one can then use the theory to accurately measure compartment size using the angular d-PFG MR at relatively low *q*-values. It should be noted that the long t_m angular d-PFG MR experiments provide an indication on what model could be used in analyzing the short t_m experiments in terms of compartment anisotropy: In the yeast cells, the Ψ-independent curves at long t_m justified the use of a spherical model to fit the data. The correspondence between the cell size obtained by non-invasive spectroscopy and invasive light microscopy is striking. Importantly, and of potential clinical relevance, is that the sizes were robustly extracted at low *q*-values, comparable with the *q*-values in which DTI is routinely performed, and using relatively weak gradients, albeit not as weak as currently allowed in the clinic. An increase of up to ~10% was demonstrated here in the signal arising from angular d-PFG experiments using gradient strengths of only 208 mT/m, from which the accurate size (5.46±0.45 μm) could be extracted, much lower than the gradients needed for performing s-PFG *q*-space MR or compared to gradients previously used to measure eccentricity of yeast cells (23). In the phantom, the modulated E(Ψ) plots at long t_m implied that the pores are anisotropic, albeit being randomly oriented. When an infinite cylinders shape was assumed for the pores in the phantom, the size extracted from angular bp-d-PFG measurements was also in very good agreement with the nominal inner diameter of 29±1 μm, and the slight deviation of from the nominal diameter can be attributed to incomplete suppression of the background gradient, despite the use of bipolar gradients (note that the line width in these specimens was very broad, around ~500 Hz). Another factor that may contribute to the slight deviation is that a temporally dependent background gradient may emerge, further complicating the cross terms between diffusion and background gradients (57). We also attempted a fit using a capped cylinders shape assumption (data not shown), and the results yielded a diameter of 27.04±0.96 μm and a length of 530.26±97.99 μm. Indeed, these results imply that the length/radius ratio is very large and justifies the use of infinite cylinders. It should be noted that the diffusion time (250 ms) was not sufficiently long to probe restriction on a ~500 μm length scale, again indicating that an infinite model should be used.

The E(Ψ) plots at t_m=0 ms also provide insight into the prevailing diffusion modes in the specimens. When restricted, non-Gaussian diffusion is the only prevalent diffusion mode in the specimen, the E(Ψ) bell-shaped dependencies should be detectable at low q-values. However, in a previous study, a controlled bi-compartmental phantom (37) was used to study the effect of a freely diffusing component on the E(Ψ) plots. In that phantom, restricted diffusion arising from water confined in microcapillaries was superimposed with

freely diffusing water. There, it was shown that at low *q*-values, free diffusion masks the bell shaped functions arising from restricted diffusion in the coherently placed cylinders, yielding flat E(Ψ) profiles; however, the bell shape in E(Ψ) reappeared at slightly higher *q*-values, when free diffusion was suppressed (37). Since the free diffusion term in the signal decay is Δ-dependent, prolonging Δ suppressed the fast component at lower q-values, and the E(Ψ) dependencies arising from the restricted component could be therefore emphasized at these lower q-values (37). Interestingly, in the yeast cells specimen the angular dependence was relatively flat up to $2q{\sim}400\ cm^{-1}$ (data not shown) and the bell-shaped dependencies emerged at slightly higher q-values. As in the bi-compartmental phantom, this low-q behavior was also diffusion time-dependent (data not shown), leading to the conclusion that indeed, the low *q* part of the signal is dominated by the attenuation arising from Gaussian diffusion, while at slightly higher *q*-values the free component is largely suppressed, accentuating the restricted component (37). Since the size measurement appear to be in excellent correspondence with cellular size obtained from microscopy, it seems that the bell shaped functions arise mostly from the intracellular space. Therefore, it seems reasonable to infer that the freely diffusing Gaussian component in the yeast specimen arises from extracellular diffusion. This distinction may become important in other cellular environments such as CNS tissues, where diffusion in the extracellular space may exhibit hindered or even restricted attributes. In this study, the effects of exchange were not considered, as there is yet no theory on exchange effects in angular d-PFG MR. However, it seems that owing to the remarkable agreement between the extracted cell diameter and the spectroscopy measurements, along with the observation that cells are spherical, that exchange effects are not very significant in this experimental setup.

It should be noted that in the *q*-space analysis, for example, the PDFs generated from the Fourier transform of E(*q*) data is fitted to a bi-Gaussian function. This analysis, which is equivalent to fitting a bi-Gaussian function to the E(*q*) data (or similar to fitting a biexponential to the E(b) data), assumes that the reconstructed propagator is truly bi-Gaussian with different Gaussians representing different geometric compartments. Therefore, the *q*-space approach differs from the method employed in analyzing the double-PFG data in that diffusion in the intracellular space is assumed to be Gaussian as well. Considering that the maximum *q*-value in single-PFG acquisitions was $1362\ cm^{-1}$ in this study, the $2\pi qa$ value, with a compartment size of a=~4 μm is greater than 1. Therefore, for a wide range of *q*-values, the Gaussianity assumption, which is expected to hold when $2\pi qa<1$ is less accurate. Despite this shortcoming of the approach, the value obtained from the analysis is in reasonable proximity to the expected value, and it is possible to attribute the deviation towards smaller sizes to the violation of the SGP approximation or to the truncation of the E(*q*) plots at $q=1362\ cm^{-1}$. It should be noted that the *q*-space analysis was not performed for the randomly oriented cylinders owing to their distribution of lengths and orientational dispersion.

Several groups began employing angular d-PFG in imaging using Mitra's theory (29) for extracting compartment sizes (35,36), despite violating the theory's limiting conditions. When Mitra's theory was used to extract the cell size, significant deviations from the nominal size were obtained owing to the violation of Mitra's limiting conditions (29). This is consistent with previous experimental findings on controlled phantoms (34), as well as with others' simulations (40,36). This deviation is expected to become more pronounced in smaller compartments; therefore, using the theoretical frameworks that take into account every experimental parameter is clearly beneficial. We did not attempt to fit the randomly oriented cylinders using Mitra's framework, since for an arbitrary orientation of the cylinder, the components of the two gradients perpendicular to the cylinder would not be equal to one another, thus violating Mitra's $G_1=G_2$ assumption (29). This was not an issue in

Ref. 34 because there, both gradients had been applied perpendicular to the walls of coherently oriented cylinders, and all experiments had employed gradients of equal strength.

Conclusions

To conclude, systems in which no ensemble anisotropy exists were investigated using conventional s-PFG and angular d-PFG NMR that was conducted using weak gradients. Accurate cellular size and shape anisotropy were measured at low *q*-values from angular d-PFG experiments in fixed yeast cells. The spherical shape of the cells was inferred at long mixing times, obviating the need to a-priori assume the compartment shape, and the sizes were extracted from experiments with t_m=0 ms, which also convey the microscopic anisotropy in the specimen. The correspondence of the extracted cellular sizes with invasive microscopy proved that the size and shape measurements were indeed accurate. These findings are promising in further applying the angular d-PFG methodologies in novel applications such as angular d-PFG MRI.

Acknowledgments

P.J.B, and E.Ö. were supported by the Intramural Research Program of the Eunice Kennedy Shriver National Institute of Child Health and Human Development, National Institutes of Health (NIH) and the Henry M. Jackson Foundation (HJF). Y.C. N.S., E.Ö., and P.J.B. were partially supported by a grant from the US-Israel Binational Foundation (BSF, grant number - 2009155). N.S. would like to gratefully acknowledge the Clore Scholar's Programme for a scholarship. The authors acknowledge Dr. Yael Roichman and Ms. Tal Maya from the School of Chemistry at Tel Aviv University for their assistance with the light microscopy.

Abbreviations

CNS	Central Nervous System
CSA	Compartment Shape Anisotropy
DTI	Diffusion Tensor Imaging
d-PFG	double-Pulsed Field Gradient
EA	Ensemble Anisotropy
ESR	Electron Spin Resonance
FWHM	Full Width at Half Maximum
PDF	Probability Distribution Function
PFG	Pulsed Field Gradient
QSI	q-Space Imaging
RBC	Red Blood Cell
s-PFG	single-Pulsed-Field-Gradient
μA	Microscopic Anisotropy

References

1. Stejskal EO, Tanner JE. Spin diffusion measurements - spin echoes in presence of a time-dependent field gradient. J Chem Phys. 1965; 42:288–292.
2. Basser PJ, Mattiello J, Lebihan D. Diffusion tensor spectroscopy and imaging. Biophys J. 1994; 66:259–267. [PubMed: 8130344]
3. Regan DG, Kuchel PW. Simulations of molecular diffusion in lattices of cells: Insights for NMR of red blood cells. Biophys J. 2002; 83:161–171. [PubMed: 12080109]

4. Kuntz JF, Trausch G, Palmas P, Mutzenhardt P, Canet D. Diffusive diffraction phenomenon in a porous polymer material observed by NMR using radio-frequency field gradients. J Chem Phys. 2007; 126:134904. [PubMed: 17430064]
5. Song YQ, Ryu SG, Sen PN. Determining multiple length scales in rocks. Nature. 2000; 406:178–181. [PubMed: 10910355]
6. Callaghan PT, Coy A, Macgowan D, Packer KJ, Zelaya FO. Diffraction-like effects in NMR diffusion studies of fluids in porous solids. Nature. 1991; 351:467–469.
7. Avram L, Assaf Y, Cohen Y. The effect of rotational angle and experimental parameters on the diffraction patterns and micro-structural information obtained from q-space diffusion NMR: implication for diffusion in white matter fibers. J Magn Reson. 2004; 169:30–38. [PubMed: 15183354]
8. Kuchel PW, Coy A, Stilbs P. NMR “diffusion-diffraction” of water revealing alignment of erythrocytes in a magnetic field and their dimensions and membrane transport characteristics. Magn Reson Med. 1997; 37:637–643. [PubMed: 9126936]
9. Pages G, Szekely D, Kuchel PW. Erythrocyte-shape evolution recorded with fast-measurement NMR diffusion-diffraction. J Magn Reson Imaging. 2008; 28:1409–1416. [PubMed: 19025949]
10. Topgaard D, Malmborg C, Söderman O. Restricted self-diffusion of water in a highly concentrated W/O emulsion studied using modulated gradient spin-echo NMR. J Magn Reson. 2002; 156:195–201. [PubMed: 12165254]
11. Feintuch A, Grayevsky A, Kaplan N, Dormann E. Diffusive diffraction of the local ESR pulse-gradient spin-echo signal in a restricted one-dimensional conductor. Phys Rev Lett. 2004; 92:156803. [PubMed: 15169305]
12. Cory DG, Garroway AN. Measurement of translational displacement probabilities by NMR - an indicator of compartmentation. Magn Reson Med. 1990; 14:435–444. [PubMed: 2355827]
13. Cohen Y, Assaf Y. High b-value q-space analyzed diffusion-weighted MRS and MRI in neuronal tissues - a technical review. NMR Biomed. 2002; 15:516–542. [PubMed: 12489099]
14. Assaf Y, Mayk A, Cohen Y. Displacement imaging of spinal cord using q-space diffusion-weighted MRI. Magn Reson Med. 2000; 44:713–722. [PubMed: 11064406]
15. Bar-Shir A, Cohen Y. High b-value q-space diffusion MRS of nerves: structural information and comparison with histological evidence. NMR Biomed. 2008; 21:165–174. [PubMed: 17492659]
16. Bar-Shir A, Duncan ID, Cohen Y. QSI and DTI of excised brains of the myelin-deficient rat. Neuroimage. 2009; 48:109–116. [PubMed: 19539038]
17. Biton IE, Duncan ID, Cohen Y. q-space diffusion of myelin-deficient spinal cords. Magn Reson Med. 2007; 58:993–1000. [PubMed: 17969109]
18. King MD, Houseman J, Roussel SA, Vanbruggen N, Williams SR, Gadian DG. Q-Space Imaging of the Brain. Magn Reson Med. 1994; 32:707–713. [PubMed: 7869892]
19. Ong HH, Wright AC, Wehrli SL, Souza A, Schwartz ED, Hwang SN, Wehrli FW. Indirect measurement of regional axon diameter in excised mouse spinal cord with q-space imaging: Simulation and experimental studies. Neuroimage. 2008; 40:1619–1632. [PubMed: 18342541]
20. Ong HH, Wehrli FW. Quantifying axon diameter and intra-cellular volume fraction in excised mouse spinal cord with q-space imaging. Neuroimage. 2010; 51:1360–1366. [PubMed: 20350604]
21. Johansen-Berg, H.; Behrens, TEJ., editors. Diffusion MRI: From quantitative measurement to in-vivo neuroanatomy. Academic Press; 2009.
22. Cory DG, Garroway AN, Miller JB. Applications of spin transport as a probe of local geometry. Polymer Preprints. 1990; 31:149–150.
23. Cheng Y, Cory DG. Multiple scattering by NMR. J Am Chem Soc. 1999; 121:7935–7936.
24. Callaghan PT, Komlosh ME. Locally anisotropic motion in a macroscopically isotropic system: displacement correlations measured using double pulsed gradient spin-echo NMR. Magn Reson Chem. 2002; 40:S15–S19.
25. Komlosh ME, Horkay F, Freldlin RZ, Nevo U, Assaf Y, Basser PJ. Detection of microscopic anisotropy in gray matter and in a novel tissue phantom using double Pulsed Gradient Spin Echo MR. J Magn Reson. 2007; 189:38–45. [PubMed: 17869147]

26. Komlosh ME, Lizak MJ, Horkay F, Freidlin RZ, Basser PJ. Observation of microscopic diffusion anisotropy in the spinal cord using double-pulsed gradient spin echo MRI. Magn Reson Med. 2008; 59:803–809. [PubMed: 18383293]
27. Blumich B, Callaghan PT, Damion RA, Han S, Khrapitchev AA, Packer KJ, Stapf S. Two-dimensional NMR of velocity exchange: VEXSY and SERPENT. J Magn Reson. 2001; 152:162–167. [PubMed: 11531375]
28. Callaghan PT, Godefroy S, Ryland BN. Use of the second dimension in PGSE NMR studies of porous media. Magn Reson Imaging. 2003; 21:243–248. [PubMed: 12850714]
29. Mitra PP. Multiple wave-vector extensions of the NMR Pulsed-Field-Gradient spin-echo diffusion measurement. Phys Rev B. 1995; 51:15074–15078.
30. Özarslan E, Basser PJ. MR diffusion-"diffraction" phenomenon in multi-pulse-field-gradient experiments. J Magn Reson. 2007; 188:285–294. [PubMed: 17723314]
31. Özarslan E, Basser PJ. Microscopic anisotropy revealed by NMR double pulsed field gradient experiments with arbitrary timing parameters. J Chem Phys. 2008; 128:154511. [PubMed: 18433239]
32. Özarslan E, Shemesh N, Basser PJ. A general framework to quantify the effect of restricted diffusion on the NMR signal with applications to double pulsed field gradient NMR experiments. J Chem Phys. 2009; 130:104702. [PubMed: 19292544]
33. Özarslan E. Compartment shape anisotropy (CSA) revealed by double pulsed field gradient MR. J Magn Reson. 2009; 199:56–67. [PubMed: 19398210]
34. Shemesh N, Özarslan E, Basser PJ, Cohen Y. Measuring small compartmental dimensions with low-q angular double-PGSE NMR: The effect of experimental parameters on signal decay. J Magn Reson. 2009; 198:15–23. [PubMed: 19186086]
35. Koch MA, Finsterbusch J. Compartment size estimation with double wave vector diffusion-weighted Imaging. Magn Reson Med. 2008; 60:90–101. [PubMed: 18421690]
36. Weber T, Ziener CH, Kampf T, Herold V, Bauer WR, Jakob PM. Measurement of apparent cell radii using a multiple wave vector diffusion experiment. Magn Reson Med. 2009; 61:1001–1006. [PubMed: 19205023]
37. Shemesh N, Özarslan E, Bar-Shir A, Basser PJ, Cohen Y. Observation of restricted diffusion in the presence of a free diffusion compartment: single- and double-PFG experiments. J Magn Reson. 2009; 200:214–225. [PubMed: 19656697]
38. Finsterbusch J, Koch MA. A tensor approach to double wave vector diffusion-weighting experiments on restricted diffusion. J Magn Reson. 2008; 195:23–32. [PubMed: 18774322]
39. Finsterbusch J. Extension of the double-wave-vector diffusion-weighting experiment to multiple concatenations. J Magn Reson. 2009; 198:174–182. [PubMed: 19268616]
40. Koch MA, Finsterbusch J. Numerical simulation of double-wave vector experiments investigating diffusion in randomly oriented ellipsoidal pores. Magn Reson Med. 2009; 62:247–254. [PubMed: 19319986]
41. Lawrenz M, Koch MA, Finsterbusch J. A tensor model and measures of microscopic anisotropy for double-wave-vector diffusion-weighting experiments with long mixing times. J Magn Reson. 2009; 202:43–56. [PubMed: 19854085]
42. Shemesh N, Özarslan E, Adiri T, Basser PJ, Cohen Y. Noninvasive bipolar double-pulsed-field-gradient NMR reveals signatures for pore size and shape in randomly oriented, polydisperse, inhomogeneous porous media. J Chem Phys. 2010; 133:044705. [PubMed: 20687674]
43. Shemesh N, Cohen Y. The effect of experimental parameters on the signal decay in double-PGSE experiments: Negative diffractions and enhancement of structural information. J Magn Reson. 2008; 195:153–161. [PubMed: 18845460]
44. Shemesh N, Özarslan E, Basser PJ, Cohen Y. Detecting diffusion-diffraction patterns in size distribution phantoms using double-pulsed field gradient (d-PFG) NMR: Theory and experiments. J Chem Phys. 2010; 132:034703. [PubMed: 20095748]
45. Aslund I, Topgaard D. Determination of the self-diffusion coefficient of intracellular water using PGSE NMR with variable gradient pulse length. J Magn Reson. 2009; 201:250–254. [PubMed: 19800273]

46. Aslund I, Nowacka A, Nilsson M, Topgaard D. Filter-exchange PGSE NMR determination of cell membrane permeability. J Magn Reson. 2009; 200:291–295. [PubMed: 19647458]
47. Malmborg C, Sjobeck M, Brockstedt S, Englund E, Söderman O, Topgaard D. Mapping the intracellular fraction of water by varying the gradient pulse length in q-space diffusion MRI. J Magn Reson. 2006; 180:280–285. [PubMed: 16571376]
48. Torres AM, Michniewicz RJ, Chapman BE, Young GAR, Kuchel PW. Characterisation of erythrocyte shapes and sizes by NMR diffusion-diffraction of water: Correlations with electron micrographs. Magn Reson Imaging. 1998; 16:423–434. [PubMed: 9665553]
49. Assaf Y, Ben-Bashat D, Chapman J, Peled S, Biton IE, Kafri M, Segev Y, Hendler T, Korczyn AD, Graif M, Cohen Y. High b-value q-space analyzed diffusion-weighted MRI: Application to multiple sclerosis. Magn Reson Med. 2002; 47:115–126. [PubMed: 11754450]
50. Biton IE, Mayk A, Kidron D, Assaf Y, Cohen Y. Improved detectability of experimental allergic encephalomyelitis in excised swine spinal cords by high b-value q-space DWI. Exp Neurol. 2005; 195:437–446. [PubMed: 16098966]
51. Assaf Y, Basser PJ. Composite hindered and restricted model of diffusion (CHARMED) MR imaging of the human brain. Neuroimage. 2005; 27:48–58. [PubMed: 15979342]
52. Assaf Y, Blumenfeld-Katzir T, Yovel Y, Basser PJ. AxCaliber: A method for measuring axon diameter distribution from diffusion MRI. Magn Reson Med. 2008; 59:1347–1354. [PubMed: 18506799]
53. Drobnjak I, Siow B, Alexander DC. Optimizing gradient waveforms for microstructure sensitivity in diffusion-weighted MR. J Magn Reson. 2010; 206:41–51. [PubMed: 20580294]
54. Codd SL, Callaghan PT. Spin echo analysis of restricted diffusion under generalized gradient waveforms: Planar, cylindrical, and spherical pores with wall relaxivity. J Magn Reson. 1999; 137:358–372. [PubMed: 10089170]
55. Beaulieu C. The basis of anisotropic water diffusion in the nervous system - a technical review. NMR Biomed. 2002; 15:435–455. [PubMed: 12489094]
56. Clark CA, Le Bihan D. Water diffusion compartmentation and anisotropy at high b values in the human brain. Magn Reson Med. 2000; 44:852–859. [PubMed: 11108621]
57. Sun PZ, Seland JG, Cory D. Background gradient suppression in pulsed gradient stimulated echo measurements. J Magn Reson. 2003; 161:168–173. [PubMed: 12713966]

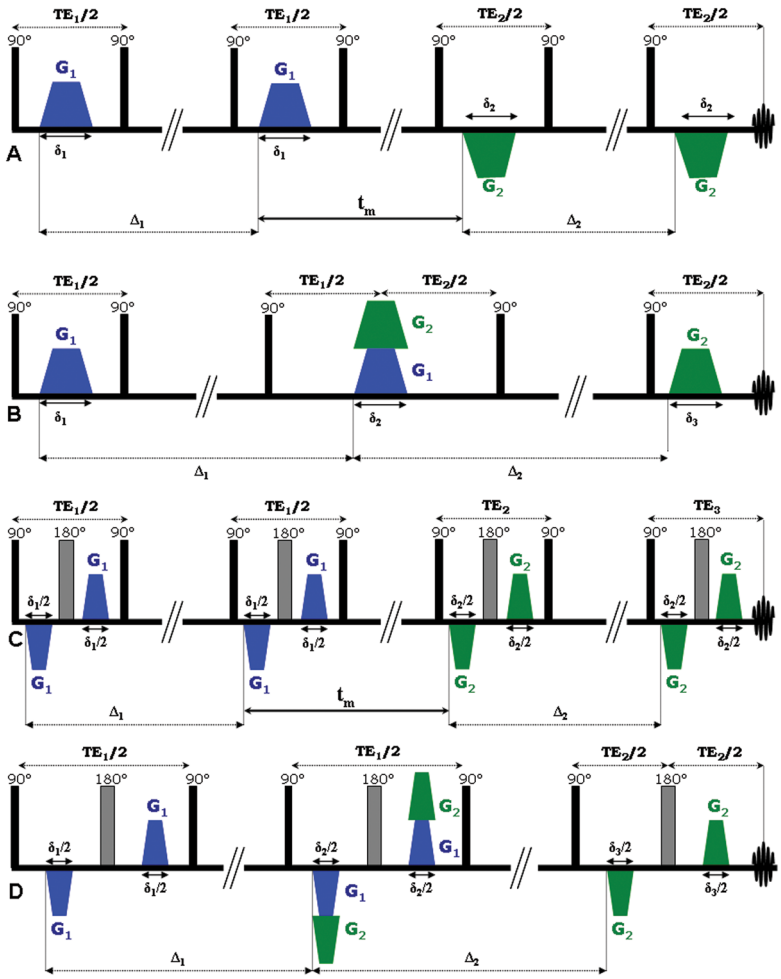

Figure 1.

Double-PFG sequences. **(A)** d-PFG sequence with finite mixing time. Note that here, the $\mathbf{G_1}$ and $\mathbf{G_2}$ are in fact applied in the same directional sense, appearing opposite only due to the pair of 90o RF pulses between the gradient pairs. **(B)** d-PFG with zero mixing time. **(C)** bp-d-PFG with finite mixing time. **(D)** bp-d-PFG with zero mixing time. Note that in the bipolar versions of the d-PFG sequences, the gradient duration is cut in half.

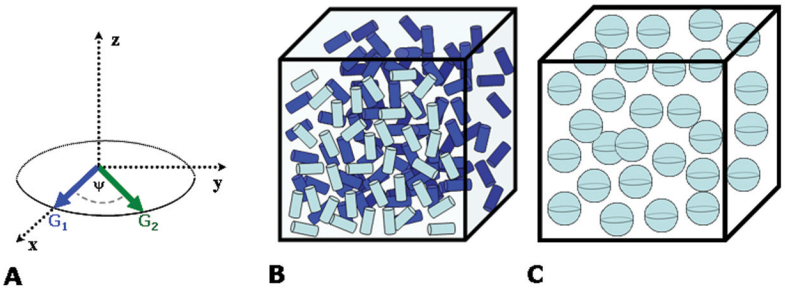

Figure 2.

Angular d-PFG methodology and orientation schemes. **(A)** The angular d-PFG MR methodology involves fixing $\mathbf{G_1}$ in a certain direction, and then performing experiments when only the orientation of $\mathbf{G_2}$ is varied relative to $\mathbf{G_1}$ along the angle Ψ. Note that in such experiments $|\mathbf{G_1}|=|\mathbf{G_2}|$, and therefore the angular d-PFG experiments are conducted at a given *q*-value. **(B)** A scheme of randomly oriented anisotropic compartments. **(C)** A scheme of spherical compartments.

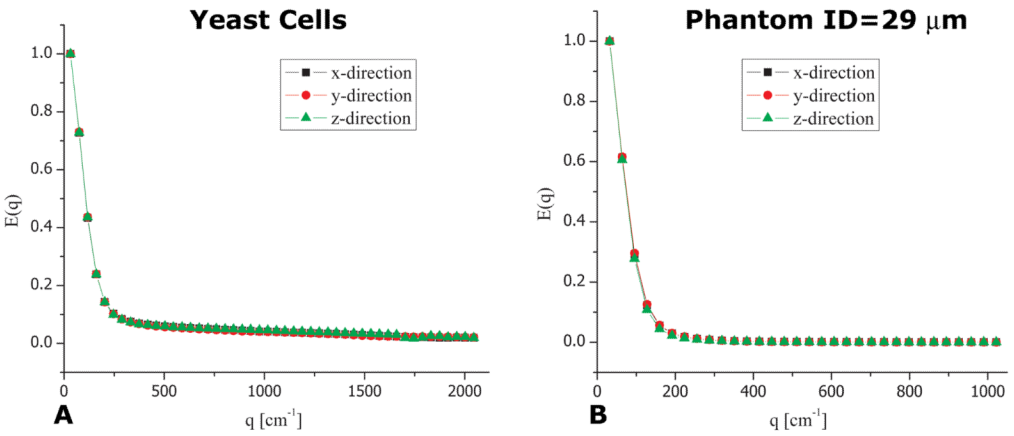

Figure 3.

bp-s-PFG experiments in yeast cells and phantoms. **(A)** bp-s-PFG experiments conducted on the fixed yeast cells with Δ=200 ms. The signal attenuation in the x-, y- and z-directions is very similar, indicating on the macroscopic isotropy of the cells. **(B)** Similar bp-s-PFG experiments conducted on the phantom comprised of randomly oriented cylinders having an ID of 29±1 μm with Δ=250 ms.

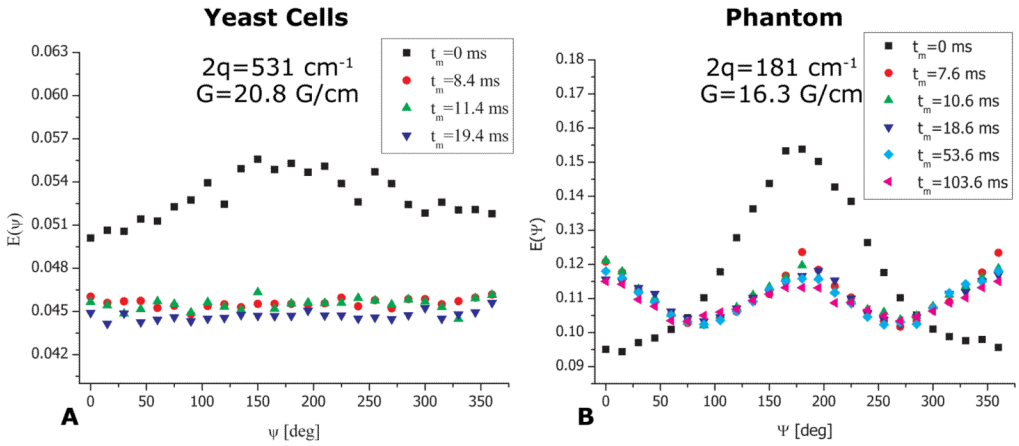

Figure 4.

bp-d-PFG experiments depicting the mixing time dependence in yeast cells and in the phantom. **(A)** bp-d-PFG experiments in yeast cells showing that with increasing mixing time, a flat angular dependence is observed, conveying the spherical morphology of the cells. **(B)** bp-d-PFG conducted in the phantom with randomly oriented cylindrical compartments with ID=29±1 μm. A qualitatively different t_m-dependence can be seen, from which it can be inferred that the compartments are anisotropic, despite being completely randomly oriented. Note the pronounced modulations in E(Ψ) arising from compartment shape anisotropy.

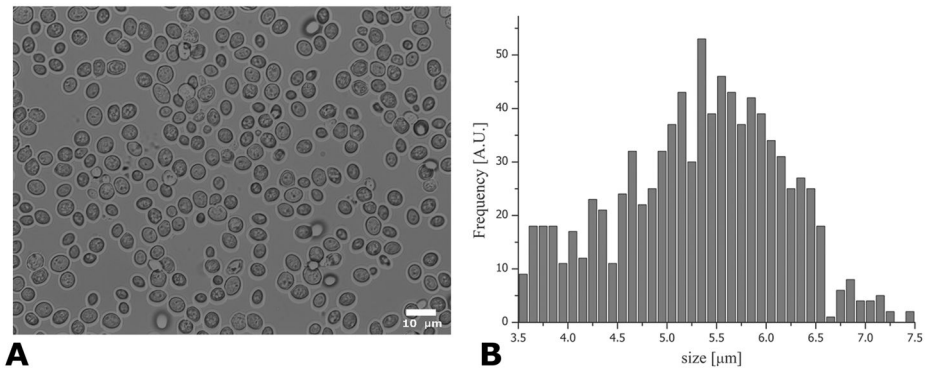

Figure 5.

Microscopy and quantification of cell size. **(A)** Representative light microscope image showing that the majority of cells are indeed relatively spherical. **(B)** Quantification of ~900 individual yeast cells resulted in a cell size of 5.32±0.83 μm.

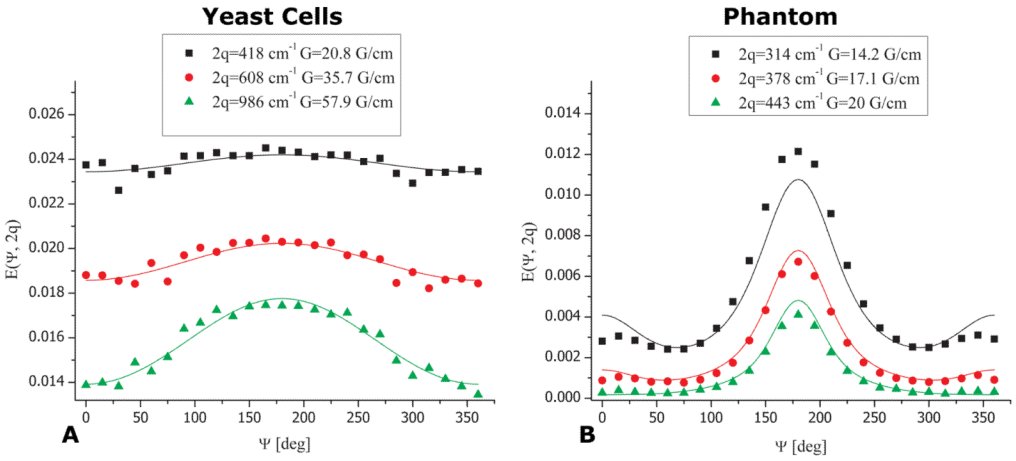

Figure 6.

Quantifying cell size from the non-invasive angular d-PFG MR. **(A)** d-PFG experiments (symbols) and theoretical fitting (lines) in the yeast cells show excellent agreement. The compartment size was extracted blindly and was found to be 5.46±0.45 μm. **(B)** bp-d-PFG experiments (symbols) and theoretical fitting (lines) in the phantom with ID=29±1 μm. The size that was extracted was 27.08±0.22 μm, in good agreement with the nominal inner diameter. The slight deviation from the nominal ID is likely due to incomplete suppression of background gradients.